Published OnlineFirst July 24, 2019; DOI: 10.1158/1535-7163.MCT-19-0185

Small Molecule Therapeutics

Molecular Cancer Therapeutics

Specific RITA Modification Produces Hyperselective Cytotoxicity While Maintaining *In Vivo* Antitumor Efficacy

Brian D. Peyser[1], Ann Hermone[2], Joseph M. Salamoun[3], James C. Burnett[1,3], Melinda G. Hollingshead[4], Connor F. McGrath[2], Rick Gussio[1], and Peter Wipf[3]

Abstract

The preclinical antitumor agent RITA (2,5-bis[5-hydroxymethyl-2-thienyl] furan, NSC 652287), an analog of the natural product α-terthiophene, failed during the development phase due to acute pulmonary toxicity in animal models. A series of synthetic modifications to RITA's heterocyclic scaffold resulted in activity ranging from broadly cytotoxic to highly selective. In the NCI 60-cell line screen, these "hyperselective" agents (e.g., imatinib) are rare. A selectivity index (SI) was developed to quantify this desirable feature, which is 20 for imatinib, whereas RITA's SI is only 0.10. One of the described hyperselective RITA analogs (SI = 7.9) completely lost activity in the presence of a known SULT1A1 inhibitor. These results, coupled with previous evidence that RITA is a SULT1A1 substrate, suggest that carbinol modification by a sulfate leaving group and subsequent formation of a reactive carbocation may explain RITA's broad cytotoxicity. Although SULT1A1 expression is required for susceptibility, hyperselective analogs exhibited reduced association of activity with *SULT1A1* mRNA expression compared with RITA, apparently requiring some additional target(s). In support of this hypothesis, there is a strong correlation ($P < 0.01$, $r = 0.95$) between quantum mechanically calculated energy barriers for carbocation formation from sulfonated analogs and SI, indicating that hyperselective RITA analogs generate reactive carbocations less readily after sulfate activation. Importantly, narrowing the cytotoxicity profile of RITA did not eliminate its analogs' *in vivo* antitumor activity, as several new hyperselective agents, NSC 773097 (**1**), 773392 (**2**), and 782846 (**6**), displayed impressive activity against A498 xenografts in mice.

Introduction

The screening of compounds related to the natural product α-terthiophene (1) in the NCI 60-cell-line anticancer drug screen (NCI-60; ref. 2) resulted in the discovery of heterocyclic triads with antitumor activity (3–9). Specifically, the heterocyclic triad 2,5-bis(5-hydroxymethyl-2-thienyl) furan—Cancer Chemotherapy National Service Center number (NSC) 652287—was shown to have promising potency against a number of cancer cell lines in the NCI-60 panel (4). NSC 652287 did not impact all cancer cell lines equally, showing the greatest activity against the renal carcinoma line A498. In an effort to explain this differential activity, a research group from the NCI studied the accumulation, retention, and metabolism of NSC 652287 in 4 renal carcinoma cell types (4). Lower 50% growth inhibition (GI_{50}) values for NSC 652287 correlated with higher accumulation, lower retention, and faster metabolism. The observation that faster metabolism correlated with higher potency provided an early indication that NSC 652287 may act as a prodrug.

Several mechanisms of action have been suggested for the anticancer activity of NSC 652287, including DNA/protein cross-linking (10) and alteration of HIF1A expression (11). Despite a lack of conclusive evidence (12), the most widely accepted mechanism has been the interaction between NSC 652287 and the N-terminal domain of TP53 to block TP53–MDM2 complex formation, inspiring the acronym Reactivation of p53 and Induction of Tumor cell Apoptosis (RITA; refs. 13, 14). RITA was subsequently shown to influence other TP53-mediated activities in the presence of wild-type and mutant *TP53* (15–20). Ascribed activities include the regulation of pro- and antiapoptotic genes, autophagy induction, the downregulation of MYC, cyclin E, and β-catenin oncogene expression, inhibition of the PI3K/Akt signaling pathway, and inhibition of TXNRD1. However, recent work indicates that RITA's mechanism is inconsistent with TP53–MDM2 binding interference, and that it likely induces DNA damage (21) as originally suggested (4, 10).

Structure–activity relationship studies for RITA analogs indicate the importance of carbinol moieties attached to the terminal aromatic heterocycles for activity (22). Carbinol-substituted polycyclic aromatic hydrocarbons, such as 1-hydroxymethylpyrene (HMP), have been shown to be activated through sulfate addition by SULT1A1 (23–26). This activation is characterized by

[1]Computational Drug Development Group, Developmental Therapeutics Program, Division of Cancer Treatment and Diagnosis, NCI, Bethesda, Maryland. [2]Computational Drug Development Group, Developmental Therapeutics Program, Leidos Biomedical Research Inc., Frederick National Laboratory for Cancer Research, Frederick, Maryland. [3]Department of Chemistry, University of Pittsburgh, Pittsburgh, Pennsylvania. [4]Biological Testing Branch, Developmental Therapeutics Program, Division of Cancer Treatment and Diagnosis, NCI, Bethesda, Maryland.

Note: Supplementary data for this article are available at Molecular Cancer Therapeutics Online (http://mct.aacrjournals.org/).

Corresponding Author: Brian D. Peyser, NCI, Riverside 5 Suite 400, 8490 Progress Dr, Frederick, MD 21701. Phone: 301-624-1262; E-mail: brian.peyser@nih.gov

Mol Cancer Ther 2019;18:1765–74

doi: 10.1158/1535-7163.MCT-19-0185

Published OnlineFirst July 24, 2019; DOI: 10.1158/1535-7163.MCT-19-0185

modification of the aromatic carbinol with a sulfate that is subsequently eliminated, forming a stabilized benzylic carbocation. The carbocation species is likely the reactive group accounting for the mutagenetic effects of HMP (24). A similar mechanism resulting in DNA/protein crosslink formation was suggested for aminoflavone (NSC 686288). Aminoflavone must undergo hydroxylation by cytochrome P450 enzymes prior to its proposed activation by SULTs (27).

The dependence of RITA on TP53 for activity was based on its differential activity in HCT116 and HCT116 $p53^{-/-}$ cells (13). More recently, it was shown that HCT116 $p53^{-/-}$ cells lose SULT1A1 protein expression, which explains their insensitivity to N-benzyl indole carbinols (28). Just as HCT116 $p53^{-/-}$ cells become insensitive to N-benzyl indole carbinols due to loss of SULT1A1 expression, RITA's activity is likely to be dependent on SULT1A1 rather than TP53, which is consistent with recent evidence that TP53 expression is not required for RITA activity (21). Other recent data indicate that the activity of RITA correlates with *SULT1A1* mRNA expression over a large set of the Cancer Cell Line Encyclopedia (29), as well as protein expression in a subset of those lines, and that SULT1A1 modifies RITA *in vitro* (30). These results suggest that the same mechanism of prodrug activation by SULT1A1 observed for HMP, aminoflavone, and N-benzyl indole carbinols also applies to RITA's anticancer activity.

Following the discovery of RITA's preclinical antitumor efficacy, a drug development program was initiated by the Developmental Therapeutics Program (DTP) at NCI. However, at levels similar to efficacious doses observed in mouse xenografts of human cancer cell lines (4), RITA caused pulmonary edema during rat, dog, and monkey toxicity studies, and the program was terminated. Hence, any further development of this chemotype necessitates the generation of analogs with significantly reduced pulmonary toxicity.

At the time of the RITA studies, the accepted paradigm for prioritizing potential new anticancer agents focused on the identification of broadly cytotoxic molecules. With the advent of precision medicine and knowledge that cancer specific therapeutics such as imatinib (Gleevec) can be used in the clinic with fewer adverse side effects, the concept of selectively targeting more finely grained cancer types is now widely viewed as a desirable route for drug development. With respect to RITA, we hypothesize that the pulmonary edema observed in multiple mammals was due to nonspecific biological activities of the molecule, such as the tendency to form DNA/protein crosslinks, and that these adverse effects can be reduced with a more cell-selective analog. When considering the cytotoxic activities of compounds in general, this hypothesis predicts that increased cell specificity in a cancer cell line screen can be a marker for reduced off-target or general cytotoxic effects. Correspondingly, if the molecules/metabolites that cause *in vivo* toxicity are present in the *ex vivo* cell line screen, this specificity may also serve as a marker for toxicity in animals. Following this logic, for some chemotypes, it may be possible to maintain efficacy while reducing toxicity by generating more cell-selective agents.

To gain a better understanding of the structural features of RITA affecting A498 cell-selectivity, we previously synthesized several novel analogs (Fig. 1; ref. 5). In this report, using data obtained from the NCI-60 cell screen, we describe the cell line selectivity profiles of these compounds. Specifically, we present a selectivity index (SI) calculation that summarizes cell selectivity in the context of NCI-60 5-dose data, and we examine the tendency of metabolites of RITA and its analogs to form carbocations using quantum mechanics— an attribute expected to be associated with nonspecific DNA/protein crosslinking and broad-scale cytotoxicity. Finally, the SI helped to identify the most attractive tumor-specific leads for *in vivo* examination, and we show that the potent activity of the RITA chemotype in A498 mouse xenograft models can be maintained while nonspecific cytotoxicity is reduced.

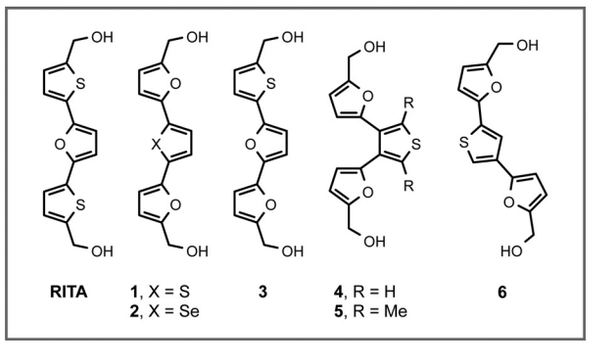

Figure 1.
RITA and analogs. Structures featuring variations of the heterocyclic triads.

Materials and Methods

Cell screening

NCI-60 5-dose screening was performed by DTP as described on the DTP website (31). One-dose assays were also performed as described on the website, except that doses were chosen as indicated *infra*, and compounds were combined at the indicated concentrations.

Microarray analysis

NCI-60 mRNA expression values were obtained from Affymetrix HG-U133 Plus 2 microarrays with NCBI GEO accession number GSE32474. The data were gcrma-normalized using the justGCRMA function and the optimize.by = "memory" option in R/Bioconductor version 3.6 (32, 33), and then each probeset was summarized using the median $\log_2$ expression value within each cell line. Probeset 203615_x_at was chosen to represent transcript expression from the 3 available *SULT1A1* probesets.

Cell line SI

Concentration responses for 5-dose NCI-60 assays were individually obtained for each experiment conducted, and SI was calculated for each substance tested at a given concentration range. Area under the percent growth curve (AUC) values were obtained for each cell line in each individual experiment, and summarized as the median AUC for each cell line among all experiments performed at that concentration range. Only cell lines with at least 2 AUC values were retained. The SI was defined as the statistical metric excess kurtosis of the AUC distribution. Excess kurtosis is zero for a Gaussian distribution, whereas rare, extreme values result in a positive excess kurtosis. SI calculations were performed in R version 3.4.4 (34) using the e1071 package version 1.6.8 for measurement of excess kurtosis. Kurtosis values were determined using the textbook estimate (type 1 in e1071), where it is defined as 3 less than the 4th moment divided by the squared second moment.

Published OnlineFirst July 24, 2019; DOI: 10.1158/1535-7163.MCT-19-0185

Statistical analysis

All statistical analyses were performed in R version 3.4.4 (34). Correlative measures were performed using a 2-sided test of Pearson's product moment correlation. Regression analyses were performed with linear models, and the adjusted R^2 value was used to estimate the GI_{50} variance accounted for by $\log_2$ *SULT1A1* expression. Kaplan–Meier survival analysis was performed in R using the survival package version 2.41.3 (35).

Quantum mechanics

To calculate barrier heights, as well as the transition states between reactants and products, a reasonably accurate estimation of energy for a self-consistent electron disposition of the molecules is required. This necessitates utilization of quantum mechanics. Among the different levels of quantum mechanics methods available, density functional theory has been found to be both adequate and tractable. This is especially true when a large trajectory ($N = 1{,}000$) of transition states is used. We used the DMol software in the Materials Studio Software suite for transition state barrier height calculations (36). For each barrier, the initial product and reactant structures were built and optimized using the MM2 force field. The reactant structure was defined as the ligand with a sulfate group added to one carbinol. The sulfate was added to the thiophene ring carbinol of compound **3** [i.e., ({5-[5′-(hydroxymethyl)-[2,2′-bifuran]-5-yl]thiophen-2-yl} methoxy)sulfonic acid], and to the 4-substituted side of compound **6** [i.e., [(5-{5-[5-(hydroxymethyl)furan-2-yl]thiophen-3-yl}furan-2-yl)methoxy]sulfonic acid]. The products were defined as the carbocation formed from breaking the carbon-oxygen bond, and the free sulfate group. The structures were optimized using the PW91 functional (37) to the fine level (energy difference of 0.00001 Ha, a maximum force of 0.002 Ha/Å and a maximum displacement of 0.005 Å).

The 1,000 frame trajectory connecting the reactant and product was generated using the "reaction preview" tool in Materials Studio, and was used to perform transition state searching, which geometrically interpolates between the reactant and product structures to generate a trajectory. To locate a transition state, the complete linear synchronous transit/quadratic synchronous transit (complete LST/QST) method was used. This method (38) uses LST to locate a maximum energy structure along the trajectory, refines this point using constrained minimization, then performs another LST search to locate another maximum followed by another minimization. The process is repeated until a transition state is identified. The transition state searches were performed to a tolerance of 0.01 Ha/Å using the BP functional (39). The structures of the products and reactants were both optimized to a tolerance of 0.002 Ha/Å. After locating a transition state, the vibrational frequencies were calculated to ensure that there was only one imaginary frequency present. This transition state structure corresponded to the sulfate bond breaking. The transition state was then optimized using the Newton–Raphson method (40) to estimate the final barrier height.

Xenograft studies

Subcutaneously implanted xenografts were established as reported previously (41, 42). Briefly, A498 cells (NCI-DTP Catalog no. A498, RRID:CVCL_1056) were grown *in vitro* and inoculated into a cohort of donor mice. The resulting tumors were serially passaged in mice and used for the studies reported herein at *in vivo* passage six. Tumors were monitored and the mice were staged and randomized into treatment groups when average tumor size was 125 mg. Compounds **1** and **2** were prepared as solutions in 100% DMSO (Burdick & Jackson). Beginning on day 17 postimplantation, treatment was administered once daily for 5 days, once every second day 3 times, or once every 4th day 3 times, repeated once, by the intraperitoneal route using a dose volume of 1 μL of a 200 mg/mL solution per gram of body weight. Vehicle controls were treated with 1 μL of 100% DMSO/g body weight once daily on days 17 to 21, 27, 31, and 35 postimplantation. Tumor growth and body weights were monitored 2 to 3 times per week using electronic calipers and balance. Data were collected electronically via Study Director software (Studylog Systems, Inc.). Tumor weights were calculated from the caliper measurements using the formula for a prolate ellipsoid: tumor weight (mg) = (tumor length (mm) × tumor width $(mm)^2)/2$. Mice were removed from the treatment protocol when the average of tumor length and width exceeded 15 mm.

The Frederick National Laboratory for Cancer Research is accredited by the Association for Assessment and Accreditation of Laboratory Animal Care (AAALAC) International and follows the Public Health Service Policy for the Care and Use of Laboratory Animals. Animal care was provided in accordance with the procedures outlined in the "Guide for the Care and Use of Laboratory Animals" (43). All animal studies were conducted under an approved Institutional Animal Care and Use Protocol.

Xenograft experiments for compound **6** were performed by ChemPartner according to an Institutional Animal Care and Use Committee–approved protocol, following the guidance of AAALAC International. A498 cells (ATCC Catalog No. HTB-44, RRID:CVCL_1056, Lot 58033335) were grown *ex vivo* as a monolayer culture in EMEM medium supplemented with 10% FBS, 100 U/mL penicillin, and 100 μg/mL streptomycin, at 37°C in an atmosphere containing 5% CO_2 in air. Tumor cells were subcultured twice weekly by trypsin-EDTA treatment. Cells in exponential growth phase were harvested and counted for tumor inoculation. Female 6 to 7 weeks old, 19 to 21 g BALB/c nude mice (Lingchang Biotechnology Company Ltd.) were kept in individual ventilation polycarbonate cages, 4 or 5 per cage, at 20 to 26°C, 40% to 70% humidity, with sterile corn cob bedding, water, and dry granule food. Mice were inoculated subcutaneously with 1×10^7 cells, and dosing began after 20 days, when average tumor weight reached 159 mg.

Mice were randomly assigned to treatment and vehicle control groups of 8 mice each. The control group was scheduled to receive 1 μL/g body weight of 100% DMSO, and the treated group schedule was 1 μL/g of a 200 mg/mL transparent solution of **6** in 100% DMSO, intraperitoneally, once daily for 5 days. Tumor sizes were measured in 2 dimensions using a caliper, and the weights were expressed in mg using the formula: $0.5 \times l \times w^2$, where l and w are the longest and shortest diameters (in mm) of the tumor, respectively. Body weights were also measured. Animals were routinely monitored for effects on normal behavior, such as mobility, food and water consumption, body weight gain/loss, eye/hair matting, and any other abnormal effect. Mice that exhibited weight loss of 8% to 15% relative to treatment start were given half of the planned dose, and those exceeding 15% weight loss were not dosed as scheduled. All treated mice exceeded 8% body weight loss on the 4th and 5th days of dosing, resulting in 100 mg/kg doses (0.5 μL/g body weight), except for 1 mouse which exceeded 15% body weight loss on the 5th day. That mouse received no dose on day 5, and was instead dosed 200 mg/kg on

Published OnlineFirst July 24, 2019; DOI: 10.1158/1535-7163.MCT-19-0185

day 8. One mouse in the vehicle control group received a half dose (0.5 μL/g 100% DMSO) on the 4th and 5th days due to body weight loss exceeding 8%.

Treatments were compared with vehicle control xenografts using Kaplan–Meier analyses for time to event, based on the definition reported by Houghton and colleagues (44). Briefly, events were defined as quadrupling of the tumor size. Time to event was interpolated using the formula:

$$t_x = \lceil t_1 + (t_2 - t_1)\ln(V_e/V_1)/\ln(V_2/V_1) \rceil$$

where t_x is the interpolated day at which tumors at least quadrupled, t_1 the lower observation day that brackets the event, t_2 the upper observation day that brackets the event, V_1 the tumor volume at t_1, V_2 the tumor volume at t_2, and V_e is 4 times the initial tumor volume.

Results

Cell line SI

Although RITA provides a modest degree of selective cytotoxicity (4), in the age of precision medicine it should be possible to target restricted subsets of cancer types using "hyperselective" agents. To measure cell line hyperselectivity, we generated the SI by calculating excess kurtosis for the distribution of area under the growth percent versus log concentration curve (AUC) values for each cell type in 5-dose NCI-60 panels (Fig. 2). SI values were calculated for 11,524 public domain compounds tested at least twice in NCI-60 5-dose screens (Supplementary Table S1). The distribution of SI values has a median of 0.39 with a scaled median absolute deviation (MAD) of 1.2, and a long right tail reaching a maximum of 62 (Fig. 2). The SI is large for compounds that have much lower AUC for a small number of cell lines (selective cytotoxicity), or compounds with much higher AUC for a small number of cell lines (selective resistance). The SI is close to 0 for compounds with a pattern of cytotoxicity that approaches a normal distribution. Negative SI values are possible for extremely flat distributions, with a minimum of negative 2. Nontargeted chemotherapeutic agents—for example, fluorouracil (NSC 19893; SI = 0.45), cisplatin (NSC 119875; SI = 1.4), cladribine (NSC 105014; SI = 1.5), and gemcitabine (NSC 613327; SI = 0.29)—tend to exhibit SI values close to 0 (Supplementary Table S1). In contrast, imatinib, which specifically targets cells dependent on the BCR-ABL1 translocation, present among NCI-60 cell lines only in K562, exhibits a very high SI (Table 1).

When calculating SI for many screened compounds, occasionally a single cell line appears sensitive to a compound, whereas other cell lines are insensitive. When this result is not repeated in subsequent screens, it is assumed that the single response is a result of experimental error or noise. For example, NSC 85262 (SI = 32) was tested twice in the NCI-60 screen, and one test showed potent cytotoxicity only in the HL-60(TB) cell line,

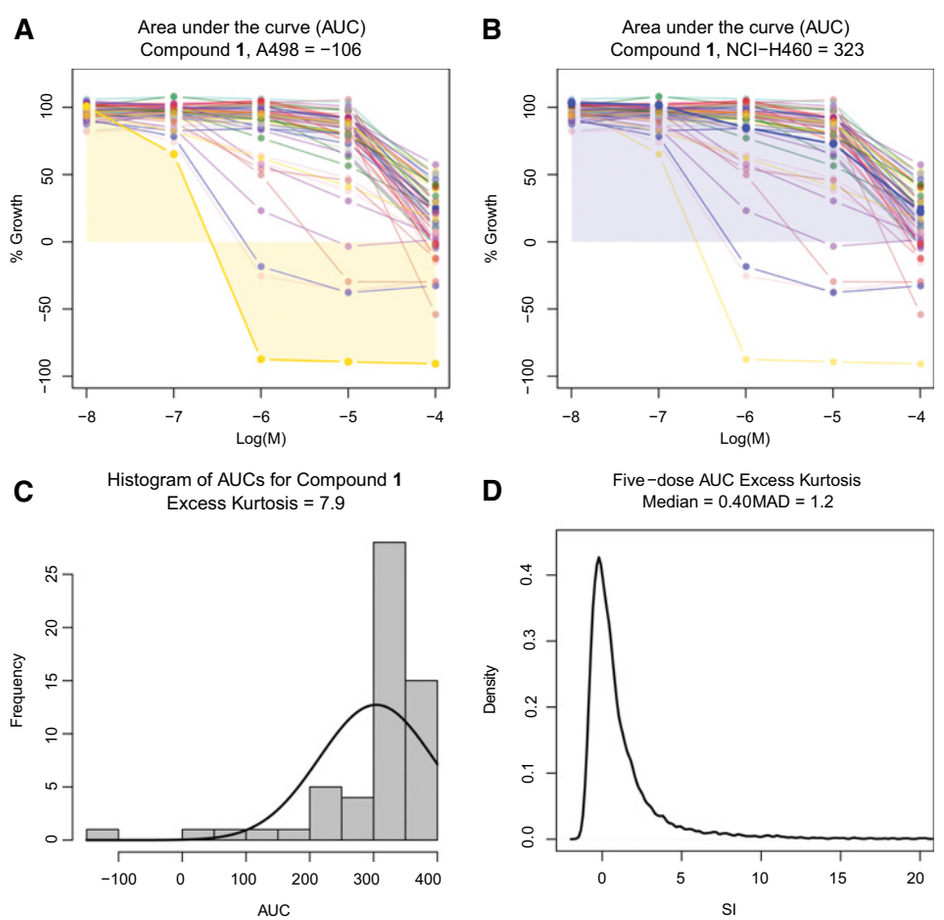

Figure 2.
Development of the SI. **A** and **B,** AUC is calculated for each cell line with data from 2 or more experiments. Dose–response for percent growth of all available cell lines from NCI-60 assays for **1** are shown, with curves colored by panel (breast cancer, pink; CNS cancer, gray; colon, green; leukemia, red; melanoma, India red; non–small lung, blue; ovarian, purple; prostate, turquoise; and renal, yellow). AUC for the renal cancer line A498 is indicated with yellow shading (**A**), and AUC for the non–small lung cancer line NCI-H460 is indicated with blue shading (**B**). **C,** Each compound's SI is the excess kurtosis for the distribution of AUC values. Kernel density of a normal distribution matching the mean and standard deviation of the histogram is shown with a black line. **D,** Kernel density for SI values of public compounds shows a long right tail, indicating very few hyperselective agents.

Published OnlineFirst July 24, 2019; DOI: 10.1158/1535-7163.MCT-19-0185

Table 1. Growth inhibition of selected cancer cell lines in the NCI-60 assay and associated SI

		GI_{50} (μmol/L)[a]									
	NSC	**A498**	**K562**	**NCI-H460**	**CAKI-1**	**TK-10**	**RXF 393**	**786-0**	**ACHN**	**SN12C**	**SI**
RITA	652287[b]	0.016	0.60	0.056	0.012	0.029	0.58	5.2	20	6.8	0.10
1	773097[c]	0.13	31	29	37	3.9	57	>100	39	67	7.9
2	773392[c]	0.17	38	73	>100	>100	>100	>100	>100	>100	8.2
3	777196[c]	0.014	6.1	2.0	5.0	0.29	13	98	52	63	3.6
4	777422[c]	0.016	7.0	1.3	5.0	>100	21	34	>100	>100	4.5
5	778301[c]	0.020	0.62	0.12	1.2	0.15	0.32	7.2	64	97	0.24
6	782846[c]	0.018	12	9.7	41	0.64	80	69	44	89	8.8
Imatinib	743414[b]	22	0.024	16	34	27	15	16	25	33	20

[a]GI_{50} values for all cell lines are provided in the Supplementary Information.
[b]NCI-60 data for NSC 652287 ($n = 7$) and 743414 ($n = 2$) are accessible online at https://dtp.cancer.gov.
[c]$n = 2$.

whereas in a second test no inhibition of HL-60(TB) occurred (Supplementary Fig. S1). For hyperselective agents identified in a single NCI-60 assay, we found that only approximately 5% displayed hyperselectivity in subsequent screens. Therefore, we also performed a robust SI calculation, choosing the AUC value closest to 100% growth for each cell line rather than the median value (which is identical to the mean value for the overwhelming majority of compounds that were screened fewer than 3 times). This robust method indicated that hyperselective agents are even more rare (median = 0.36; MAD = 1.0; maximum = 52) than the first calculation suggested (Supplementary Fig. S1; Supplementary Table S1). This method produced a robust SI of −0.91 for NSC 85262 by discounting the spurious result. However, even with the robust technique, data errors can produce inflated SIs. Among the top 10 public compounds by robust SI, only 3 produced consistent hyperselectivity upon close examination of their individual NCI-60 dose–response curves. Because experimental data for the described RITA analogs do not exhibit this type of spurious result, and because choosing the curve closest to no effect significantly biases the AUC distribution, we used the nonrobust method here.

NCI-60 screen results

RITA, which features a heterocyclic triad core with 2 terminal thiophenes and a central furan (Fig. 1), demonstrated a GI_{50} of approximately 16 nmol/L against A498, with broad cytotoxicity across multiple cell lines (Table 1; Supplementary Fig. S2), with 65 of 69 tested cancer cell lines exceeding total growth inhibition. As with non-target–specific chemotherapeutics, RITA has a low SI (0.10; Table 1). It is noteworthy that the renal cell line A498 was among the top 2 most sensitive cell lines (by GI_{50} value) for all RITA analogs described here. Placing a thiophene or a selenophene in the center of the triad with 2 terminal furan rings in compounds **1** and **2**, respectively, resulted in approximately 10-fold lower potency against A498 compared with RITA, but much higher SIs of 7.9 and 8.2 (Table 1). Interestingly, analog **3**, a sequence isomer of **1**, with a thiophene ring on one terminus of the triad and furans as the central and opposite terminus heterocycles, provided A498 cytotoxicity that was equipotent to RITA, but with intermediate selectivity (SI = 3.6; Table 1). Changing the triad geometry by altering the furan substitution positions to carbons 3 and 4 on the central thiophene in analogs **4** and **5** resulted in potency and selectivity similar to **3** and RITA, respectively—despite the incorporation of terminal furans as opposed to thiophenes. Therefore, repositioning the terminal furans in **4** caused a decrease in SI compared with **1**, and the addition of electron-donating methyl groups on the central aromatic thiophene in **5** further reduced the SI (Table 1). Alternate repositioning of the furans to carbons 2 and 4 of the central thiophene provided analog **6**, which was found to have A498 cytotoxicity comparable to that of RITA, but a high SI comparable to **1** and **2**. Hence, it is evident from these data that changes to the heterocyclic triad core of RITA result in different patterns of tumor cell line cytotoxicity and selectivity, and that an increase in selectivity can be accomplished without compromising potency.

SULT1A1 dependence

The activity of RITA exhibits strong association with baseline *SULT1A1* gcrma-normalized $\log_2$ mRNA expression (Fig. 3), with 62% of variance accounted for in the NCI-60 screen ($R^2 = 0.62$; $P < 0.01$; $F = 96$, 57 degrees of freedom), and RITA was shown to be a SULT1A1 substrate (30). Therefore, we examined the effect of a known phenol sulfotransferase inhibitor on the activity of **1** in a one-dose NCI-60 cell screen. Treatment with 1 μmol/L of compound **1** resulted in a relative A498 growth of −93% (Supplementary Table S2). Cotreatment of NCI-60 cells with 1 μmol/L of compound **1** and 10 μmol/L of the known phenol sulfotransferase inhibitor 2,6-dichloro-4-nitrophenol (DCNP; ref. 45) completely abrogated activity (A498 growth +97%; DCNP alone at 10 μmol/L had no effect on growth for any cell lines). Therefore, the RITA analogs described herein are likely also SULT1A1 substrates, and are activated by sulfonate addition. In this regard, the activity of **1** is also associated with *SULT1A1* expression (Fig. 3), but with less variance accounted for ($R^2 = 0.31$; $P < 0.01$; $F = 27$, 56 degrees of freedom). Strikingly, the NCI-60 line expressing the highest levels of *SULT1A1* mRNA, NCI-H460, is resistant to **1** and other hyperselective agents, whereas it is very sensitive to RITA (Table 1; Fig. 3; Supplementary Fig. S3) and analogs with low SI (e.g., analog **5**). *SULT1A2* is tightly coexpressed with *SULT1A1* ($r = 0.97$), and DCNP is also an inhibitor of SULT1A2 (46). These indicate that although phenol sulfotransferase-mediated biotransformation is required for activity of the hyperselective analogs, it is not sufficient. Some other susceptibility must be required in sensitive cell lines/tumors for the activated molecule to exhibit its cytotoxic effects.

Quantum barrier heights

Dependence on phenol sulfotransferase for the cytotoxicity of RITA and evidence that it is a substrate for SULT1A1 indicate that RITA is most likely a prodrug activated by sulfonation, with a mechanism similar to the carbocation generation observed for HMP (24). Dependence on phenol sulfotransferase activity for the cytotoxic effects of **1** suggests that all of the active RITA analogs

Published OnlineFirst July 24, 2019; DOI: 10.1158/1535-7163.MCT-19-0185

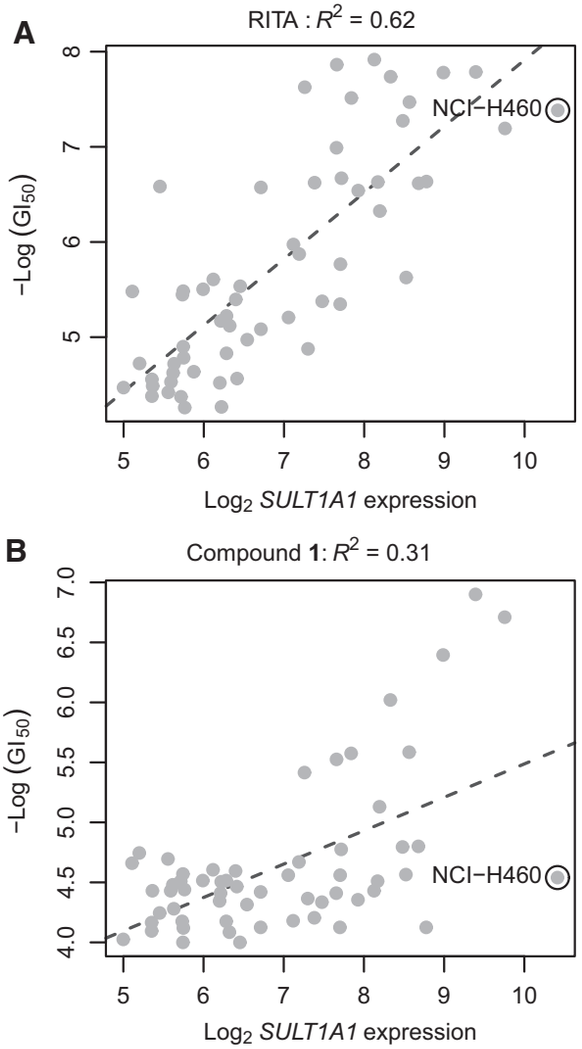

Figure 3.

Activity of RITA analogs in NCI-60 screening is associated with high *SULT1A1* mRNA expression. Sensitivity of each NCI-60 cell line is summarized as the average $-\log(GI_{50})$ across available experiments, and expression of *SULT1A1* mRNA is summarized as the median $\log_2$(expression) value for each cell line from NCI-60 Affymetrix HG-U133 Plus 2 microarrays (GSE32474). NCI-H460, the highest-expressing NCI-60 line, is indicated on each plot. **A,** RITA sensitivity is strongly associated with expression of *SULT1A1*. **B,** NCI-60 sensitivity to **1** has less variance accounted for by *SULT1A1* expression.

discussed herein are also activated by sulfonation. If the differences in activities of RITA analogs were dependent only on changes to substrate efficiency in phenol sulfotransferase, it would be expected that linear models of sensitivity versus *SULT1A1* expression would maintain R^2 values, but change slope. Instead, hyperselective analogs become less associated with *SULT1A1* expression (Fig. 3), indicating that another factor impacts susceptibility. Therefore, we examined transition state energy barriers (Fig. 4A) for formation of a carbocation from sulfonated versions of the analogs (RITA, **1**–**6**) using quantum mechanics. SI values for this series are significantly correlated ($P < 0.01$, $t = 6.7$, 5 degrees of freedom) with transition state energy barriers (Fig. 4B). Specifically, lower barriers are associated with less selective analogs, whereas higher barriers are associated with more selective analogs. For compounds with low SIs, metabolic activation to the sulfonated molecule may be sufficient for induction of DNA damage via spontaneous formation of a reactive carbocation. However, for molecules with high transition state barriers, a target-specific effect may be indicated—perhaps with carbocation formation induced by an interaction with a relevant protein binding site. A requirement among selective compounds for specific target(s) in addition to metabolic activation would explain the previously mentioned loss of activity in NCI- H460 cells despite high expression of *SULT1A1*.

Hyperselective analogs maintain *in vivo* efficacy

The development of analogs with cancer cell type hyperselectivity demonstrates that general, non-target–specific cytotoxicity can be avoided, thereby potentially reducing the pulmonary toxicity observed with RITA. However, it is important to note that while NCI-60 *ex vivo* activity against A498 was maintained with the hyperselective compounds, the *in vivo* activity of RITA may be due to its non-target–specific effects. Therefore, to verify if cell activity for the hyperselective analogs would translate to *in vivo* efficacy, we examined the reported analogs with high SI (1, 2, and 6) in A498 xenografts.

Treatment of this mouse xenograft model with hyperselective compound **1** showed impressive inhibition of tumor growth (Fig. 5) with an optimal percent test over control tumor weight (%T/C) of 11%, 24 days after treatment delivery was completed (Supplementary Fig. S4). The average relative mouse body weight decreased by about 10% over the course of treatment, but recovered once dosing was completed. Body weight increased on average, relative to the beginning of treatment, within 22 days of treatment initiation, whereas untreated animals lost weight over the course of the study due to the effects of A498 tumors. Notably, there were no drug-related deaths, and one mouse was found to be tumor free at the end of the study.

Results for selenophene analog **2** were nearly identical to **1** during the treatment schedule (Fig. 5). Optimal %T/C was 16%, 18 days after treatment was completed. Similarly, there were no drug-related deaths, significant tumor growth suppression was observed while treatment was administered, and mouse body weights recovered to pretreatment levels by day 22. However, tumor growth resumed approximately 20 days after dosing with **2** was completed, compared with over 60 days without significant tumor growth in mice treated with **1** (Supplementary Fig. S4). The effect of resumed tumor growth in mice treated with **2** was accompanied by deterioration in mouse body weight, although not to the levels observed in untreated mice. For both **1** and **2**, additional treatment schedules produced the same general pattern of antitumor efficacy (Supplementary Fig. S4).

The RITA analog with the highest SI, compound **6**, also displayed impressive activity, causing tumors to shrink an average of 26% by the 3rd day of treatment. Tumor weight remained low for the duration of the experiment (Fig. 5). Treated mice experienced body weight loss, resulting in a reduction in dose to 100 mg/kg on the 4th and 5th days of treatment. One mouse was not dosed on the 5th day, instead receiving 200 mg/kg on the 8th day. One vehicle-treated animal also experienced weight loss significant enough to result in dose reduction. This difference in treatment regimen was dictated by differences in Institutional Animal Care and Use Committee protocols, as indicated in the methods

Published OnlineFirst July 24, 2019; DOI: 10.1158/1535-7163.MCT-19-0185

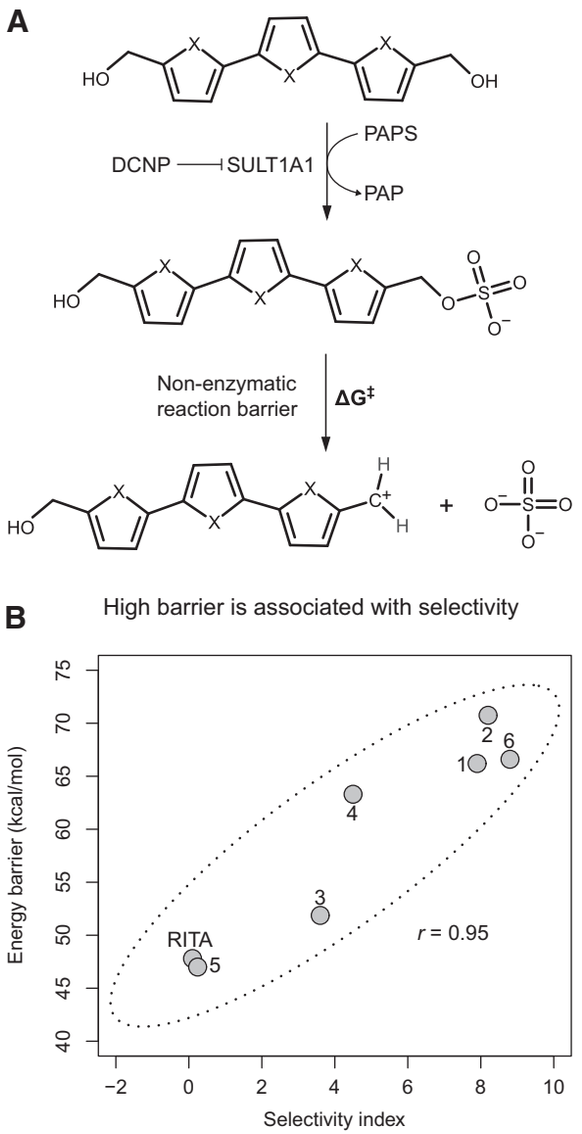

Figure 4.

Quantum mechanics–calculated barrier heights for carbocation formation are correlated with SI. **A,** Model for carbocation formation for which the energy barrier, $\Delta G^{\ddagger}$, was calculated using quantum mechanics. **B,** SI for RITA and **1** to **6** plotted with the energy barriers.

section (*vide supra*). No animals died due to treatment, and the experiment was stopped and all mice were sacrificed prior to reaching humane endpoints. Similarly to analogs **1** and **2**, mouse body weight recovered within 20 days of treatment initiation.

All compounds and treatment schedules examined resulted in significant improvement of event-free survival compared with vehicle-treated controls (Fig. 5; Supplementary Fig. S4, Bonferroni-corrected family-wise error rate <0.01).

Discussion

Motivated by the undesired *in vivo* pulmonary toxicity associated with RITA, a series of analogs with sequence order, composition, and geometry modifications to the parent's heterocyclic triad were synthesized. Testing of the compounds in the NCI-60 assay indicated that changing the arrangement of RITA's heterocyclic core enabled cell line hyperselectivity, while concomitantly retaining potent activity against renal cell line A498. Interestingly, loss of activity against the lung cell-derived line NCI-H460 suggests that these hyperselective analogs may provide the reduction in pulmonary toxicity required for advancing this chemotype through development. Furthermore, based on cell line selectivity profiles from the NCI-60 screen, we developed a new selectivity index (SI) algorithm that can be used to prioritize anticancer agents and identify attractive cell-specific lead compounds for further *in vivo* studies.

A correlation between selectivity and quantum-mechanics-calculated carbocation formation barriers for RITA and its analogs, in conjunction with empirical evidence indicating a dependence for activity on phenol sulfotransferase expression, suggests that nonspecific mechanisms involving the spontaneous formation of reactive carbocations are responsible for the DNA/protein crosslinking observed in RITA-sensitive cell lines. Consequently, the presence of this nonspecific activity is likely to be the cause of the confusing landscape of potential mechanisms of action reported for RITA. Additionally, many published comparisons of RITA's activity in sensitive cell lines versus nontransformed cells do not account for expression of phenol sulfotransferases, and therefore may miss the potential cytotoxicity of sulfotransferase-activated RITA. Interestingly, the observed increase in toxicity of RITA in higher order mammalian lungs relative to mice may be explained by the complete lack of phenol sulfotransferase activity in mouse lung cytosol, whereas mice transgenic for human *SULT1A1/2* have lung tissue capable of HMP biotransformation (47). Hence, although antitumor efficacy in mice may be possible with RITA, it is evident that analogs with increased specificity will be required for treatment of humans.

Further investigation needs to be performed to evaluate the importance of TP53 and related pathways with respect to the anticancer effects of RITA and the analogs described herein. Because RITA appears to act in a nonspecific fashion, seemingly dependent mainly on metabolic activation by phenol sulfotransferase, it is likely that previous mechanism of action studies involving this compound have been hindered by its broad activities. The generation of hyperselective analogs provides new opportunities for understanding the central mechanisms resulting in the attractive antitumor activity of this chemotype. Knowledge that sulfotransferase activation is required for the activity of RITA analogs will focus mechanistic studies on cell lines that are capable of producing the active metabolite, or on *in vitro* studies directly utilizing sulfonated derivatives. Based on our quantum mechanical calculations, it is likely that sulfonated versions of the hyperselective analogs are more stable than sulfonated RITA. Future studies will systematically examine the chemical stabilities of these sulfonated analogs.

Although analogs **1**, **2**, and **6** displayed high SI, it was not clear if this property would generally translate into lower *in vivo* activity. Therefore, these compounds were examined for efficacy in mouse xenograft models of A498. In support of our hypothesis that hyperselective analogs may be used as less toxic, yet effective alternatives to RITA, all 3 analogs retained activity against A498 xenografts, with **6** causing tumor regression at the maximum tolerated dose, and **1** producing sustained tumor growth inhibition. Therefore, while RITA causes non-target-specific effects,

Published OnlineFirst July 24, 2019; DOI: 10.1158/1535-7163.MCT-19-0185

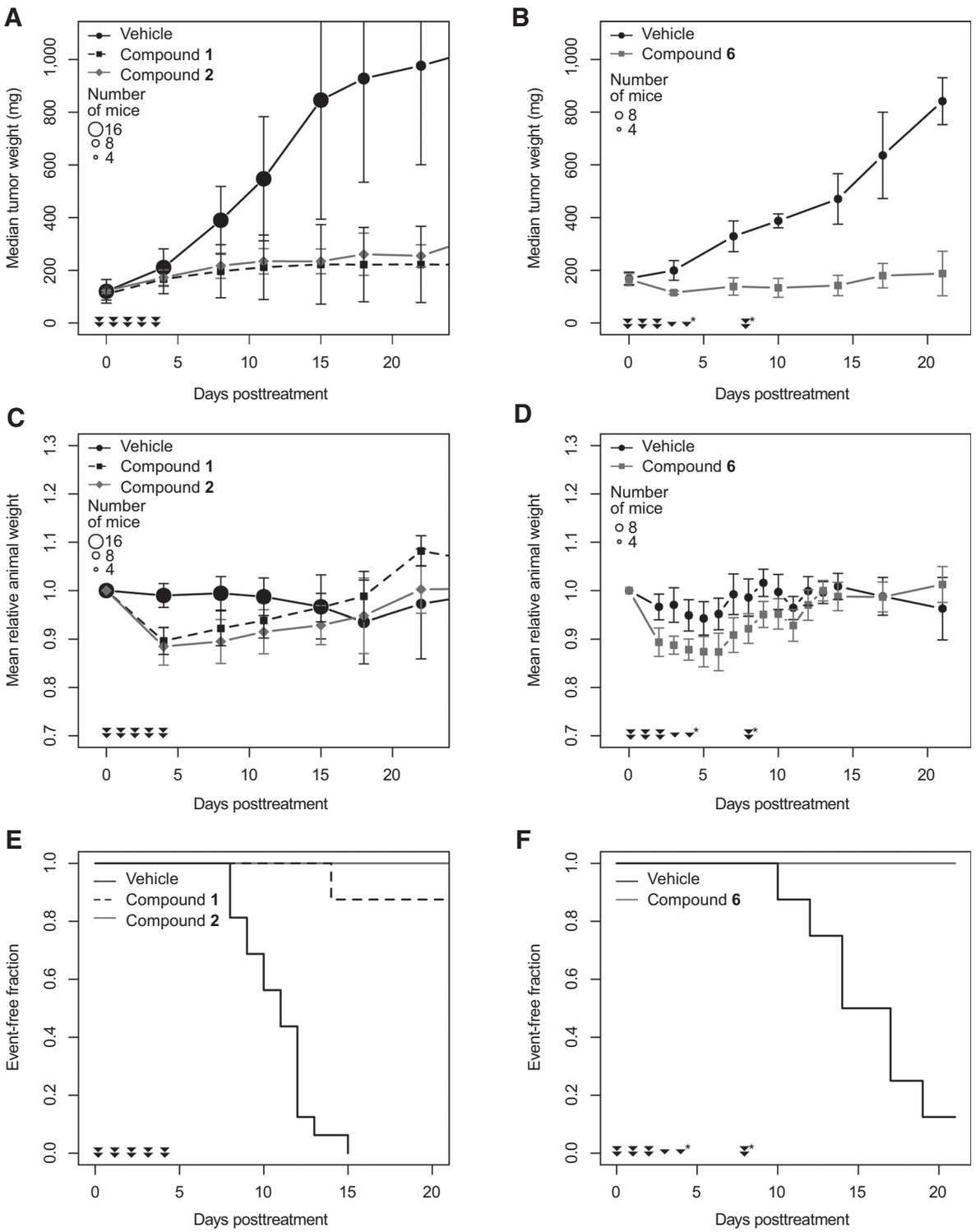

Figure 5.

Hyperselective RITA analogs maintain *in vivo* efficacy in A498 xenografts. **A** and **B**, Median tumor weight for vehicle-treated mice (black circles), and 5 daily intraperitoneal injections of 200 mg/kg (⏬) or 100 mg/kg (⏷) of **1** (black squares), **2** (gray diamonds), or **6** (gray squares). Asterisks: dose holiday for a single mouse. Bars represent one MAD. **C** and **D**, Mean mouse weight relative to treatment start. Bars represent one standard deviation. **E** and **F**, Kaplan–Meier curves indicating fraction of each group that did not reach an event, defined as quadrupling of tumor size. Symbol sizes in **A–D** represent number of mice remaining within each treatment arm, which is reduced when mice are found dead or sacrificed due to humane endpoints such as tumor size or excessive weight loss.

Published OnlineFirst July 24, 2019; DOI: 10.1158/1535-7163.MCT-19-0185

these hyperselective analogs retained a level of specific activity that is sufficient to provide significant antitumor efficacy. Future research will focus on pulmonary toxicity studies with **6** and selected analogs to further examine the hypothesis that hyperselective cytotoxicity *ex vivo* can be used as an indicator of reduced adverse effects *in vivo*, and potentially provide an enhanced therapeutic index. Additionally, as the major mechanism(s) of action are determined for the hyperselective agents, it will be important to examine these new compounds for the production of DNA/protein crosslinks in sensitive cell lines, and for other biological activities ascribed to RITA. Overall, the data generated in this study will serve to guide future work to both identify the biological target(s) and assess the therapeutic potential of **6** and similar heterocyclic triad analogs, with the goal to develop a novel cancer therapeutic.

Disclosure of Potential Conflicts of Interest

No potential conflicts of interest were disclosed.

Authors' Contributions

Conception and design: B.D. Peyser, J.C. Burnett, M.G. Hollingshead, P. Wipf
Development of methodology: B.D. Peyser, J.C. Burnett, R. Gussio, P. Wipf
Acquisition of data (provided animals, acquired and managed patients, provided facilities, etc.): A. Hermone, M.G. Hollingshead, P. Wipf
Analysis and interpretation of data (e.g., statistical analysis, biostatistics, computational analysis): B.D. Peyser, A. Hermone, M.G. Hollingshead, R. Gussio, P. Wipf
Writing, review, and/or revision of the manuscript: B.D. Peyser, J.M. Salamoun, J.C. Burnett, M.G. Hollingshead, C.F. McGrath, R. Gussio, P. Wipf
Administrative, technical, or material support (i.e., reporting or organizing data, constructing databases): B.D. Peyser, C.F. McGrath, P. Wipf
Study supervision: B.D. Peyser, P. Wipf
Other (design and synthesis of chemical compounds): J.M. Salamoun

Acknowledgments

The authors thank Jerry Collins for initiating the hyperselective program at DTP and thank David Covell and Dan Zaharevitz for comments on the manuscript. This research was supported (in part) by the Developmental Therapeutics Program in the Division of Cancer Treatment and Diagnosis of NCI (B. Peyser, M. Hollingshead, R. Gussio). This project has been funded in whole or in part with federal funds from NCI, NIH, under contract no. HHSN261200800001E. The content of this publication does not necessarily reflect the views or policies of the Department of Health and Human Services, nor does mention of trade names, commercial products, or organizations imply endorsement by the U.S. Government (to A. Hermone, C. McGrath). J. Salamoun gratefully acknowledges fellowship support by NCI (5F31CA200145). Additional discretionary funding was provided by Boehringer Ingelheim Pharmaceuticals, Inc. (to P. Wipf).

The costs of publication of this article were defrayed in part by the payment of page charges. This article must therefore be hereby marked *advertisement* in accordance with 18 U.S.C. Section 1734 solely to indicate this fact.

Received February 21, 2019; revised May 10, 2019; accepted July 16, 2019; published first July 24, 2019.

References

1. Chan GFQ, Towers GHN, Mitchell JC. Ultraviolet-mediated antibiotic activity of thiophene compounds of tagetes. Phytochemistry 1975;14:2295–6.
2. Shoemaker RH. The NCI60 human tumour cell line anticancer drug screen. Nat Rev Cancer 2006;6:813–23.
3. Juang SH, Lung CC, Hsu PC, Hsu KS, Li YC, Hong PC, et al. D-501036, a novel selenophene-based triheterocycle derivative, exhibits potent in vitro and in vivo antitumoral activity which involves DNA damage and ataxia telangiectasia-mutated nuclear protein kinase activation. Mol Cancer Ther 2007;6:193–202.
4. Rivera MI, Stinson SF, Vistica DT, Jorden JL, Kenney S, Sausville EA. Selective toxicity of the tricyclic thiophene NSC 652287 in renal carcinoma cell lines. Biochem Pharmacol 1999;57:1283–95.
5. Salamoun J, Anderson S, Burnett JC, Gussio R, Wipf P. Synthesis of heterocyclic triads by Pd-catalyzed cross-couplings and evaluation of their cell-specific toxicity profile. Org Lett 2014;16:2034–7.
6. Lin J, Jin X, Bu Y, Cao D, Zhang N, Li S, et al. Efficient synthesis of RITA and its analogues: derivation of analogues with improved antiproliferative activity via modulation of p53/miR-34a pathway. Org Biomol Chem 2012;10:9734–46.
7. Mertins SD, Myers TG, Hollingshead M, Dykes D, Bodde E, Tsai P, et al. Screening for and identification of novel agents directed at renal cell carcinoma. Clin Cancer Res 2001;7:620–33.
8. Chang C, Ashendel CL, Kim D, inventors; Purdue Research Foundation, applicant. Selenophene anti-tumor agents. World patent WO9746225. 1997 Dec 11.
9. Carter CA, Waud WR, Plowman J, Alley MA. In vivo spectrum of antitumor activity of a thiophene derivative [abstract]. In: Proceedings of the 87th American Association for Cancer Research Meeting; 1996 Apr 20–24; Washington DC. Philadelphia (PA): AACR; 1996. p. 20–4.
10. Nieves-Neira W, Rivera MI, Kohlhagen G, Hursey ML, Pourquier P, Sausville EA, et al. DNA protein cross-links produced by NSC 652287, a novel thiophene derivative active against human renal cancer cells. Mol Pharmacol 1999;56:478–84.
11. Lou JJW, Chua YL, Chew EH, Gao J, Bushell M, Hagen T. Inhibition of hypoxia-inducible factor-1α (HIF-1α) protein synthesis by DNA damage inducing agents. Jin D-Y, editor. PLoS One 2010;5:e10522.
12. Krajewski M, Ozdowy P, D'Silva L, Rothweiler UHolak T a, Grinkevich V, etal. NMR indicates that the small molecule RITA does not block p53-MDM2 binding in vitro. Nat Med 2005;11:1136–7.
13. Issaeva N, Bozko P, Enge M, Protopopova M, Verhoef LGGC, Masucci M, et al. Small molecule RITA binds to p53, blocks p53–HDM-2 interaction and activates p53 function in tumors. Nat Med 2004;10:1321–8.
14. Doggrell SA. RITA—a small-molecule anticancer drug that targets p53. Expert Opin Investig Drugs 2005;14:739–42.
15. Yang J, Ahmed A, Poon E, Perusinghe N, de Haven Brandon A, Box G, et al. Small-Molecule activation of p53 blocks hypoxia-inducible factor 1 and vascular endothelial growth factor expression in vivo and leads to tumor cell apoptosis in normoxia and hypoxia. Mol Cell Biol 2009;29:2243–53.
16. de Lange J, Verlaan-de Vries M, Teunisse AFAS, Jochemsen AG. Chk2 mediates RITA-induced apoptosis. Cell Death Differ 2012;19:980–9.
17. Jones RJ, Bjorklund CC, Baladandayuthapani V, Kuhn DJ, Orlowski RZ. Drug resistance to inhibitors of the human double minute-2 E3 ligase is mediated by point mutations of p53, but can be overcome with the p53 targeting agent RITA. Mol Cancer Ther 2012;11:2243–53.
18. Burmakin M, Shi Y, Hedström E, Kogner P, Selivanova G. Dual targeting of wild-type and mutant p53 by small molecule RITA results in the inhibition of N-Myc and key survival oncogenes and kills neuroblastoma cells in vivo and in vitro. Clin Cancer Res 2013;19:5092–103.
19. Fiorini C, Menegazzi M, Padroni C, Dando I, Dalla Pozza E, Gregorelli A, et al. Autophagy induced by p53-reactivating molecules protects pancreatic cancer cells from apoptosis. Apoptosis 2013;18:337–46.
20. Hedström E, Eriksson S, Zawacka-Pankau J, Arnér ESJ, Selivanova G. p53-dependent inhibition of TrxR1 contributes to the tumor-specific induction of apoptosis by RITA. Cell Cycle 2009;8:3584–91.
21. Wanzel M, Vischedyk JB, Gittler MP, Gremke N, Seiz JR, Hefter M, et al. CRISPR-Cas9–based target validation for p53-reactivating model compounds. Nat Chem Biol 2015;53:1–9.
22. Jiang J, Ding C, Li L, Gao C, Jiang Y, Tan C, et al. Synthesis and antiproliferative activity of RITA and its analogs. Tetrahedron Lett 2014;55:6635–8.
23. Surh Y, Blomquist JC, Liem A, Miller JA. Metabolic activation of 9-hydroxymethyl-10-methylanthracene and 1-hydroxymethylpyrene to

electrophilic, mutagenic and tumorigenic sulfuric acid esters by rat hepatic sulfotransferase activity. Carcinogenesis 1990;11:1451–60.
24. Glatt H, Werle-Schneider G, Enders N, Monnerjahn S, Pudil J, Czich A, et al. 1-Hydroxymethylpyrene and its sulfuric acid ester: toxicological effects in vitro and in vivo, and metabolic aspects. Chem Biol Interact 1994;92: 305–19.
25. Horn J, Flesher JW, Lehner AF. 1-Sulfooxymethylpyrene Is an electrophilic mutagen and ultimate carcinogen of 1-methyl- and 1-hydroxymethylpyrene. Biochem Biophys Res Commun 1996;228:105–9.
26. Glatt H. Sulfotransferases in the bioactivation of xenobiotics. Chem Biol Interact 2000;129:141–70.
27. Meng LH, Shankavaram U, Chen C, Agama K, Fu HQ, Gonzalez FJ, et al. Activation of aminoflavone (NSC 686288) by a sulfotransferase is required for the antiproliferative effect of the drug and for induction of histone gamma-H2AX. Cancer Res 2006;66:9656–64.
28. Rothman DM, Gao X, George E, Rasmusson T, Bhatia D, Alimov I, et al. Metabolic enzyme sulfotransferase 1A1 is the trigger for N-Benzyl indole carbinol tumor growth suppression. Chem Biol 2015;22: 1228–37.
29. Barretina J, Caponigro G, Stransky N, Venkatesan K, Margolin AA, Kim S, et al. The cancer cell line encyclopedia enables predictive modelling of anticancer drug sensitivity. Nature 2012;483:603–7.
30. Rees MG, Seashore-Ludlow B, Cheah JH, Adams DJ, Price E V, Gill S, et al. Correlating chemical sensitivity and basal gene expression reveals mechanism of action. Nat Chem Biol 2015;12:109–16.
31. National Cancer Institute. Discovery & Development Services | DTP [Internet]. [cited 2017 Aug 11]. Available from: https://dtp.cancer.gov/discovery_development/nci-60/default.htm.
32. Wu Z, Irizarry RA, Gentleman R, Martinez-Murillo F, Spencer F. A model-based background adjustment for oligonucleotide expression arrays. J Am Stat Assoc 2004;99:909–17.
33. Huber W, Carey VJ, Gentleman R, Anders S, Carlson M, Carvalho BS, et al. Orchestrating high-throughput genomic analysis with Bioconductor. Nat Methods 2015;12:115–21.
34. R Core Team. R: A language and environment for statistical computing. Vienna, Austria; 2017.
35. Therneau TM, Grambsch PM. Modeling survival data: extending the Cox model. 1st ed. New York, NY: Springer New York; 2000.
36. Dassault Systèmes BIOVIA. BIOVIA Materials Studio 2016. San Diego: Dassault Systèmes; 2016.
37. Perdew JP, Wang Y. Accurate and simple analytic representation of the electron-gas correlation energy. Phys Rev B 1992;45:13244–9.
38. Halgren TA, Lipscomb WN. The synchronous-transit method for determining reaction pathways and locating molecular transition states. Chem Phys Lett 1977;49:225–32.
39. Becke AD. A multicenter numerical integration scheme for polyatomic molecules. J Chem Phys 1988;88:2547–53.
40. Ermer O. Calculation of molecular properties using force fields. Applications in organic chemistry. Bond forces. Berlin, Heidelberg: Springer; 1976. p. 161–211.
41. Plowman J, Dykes DJ, Hollingshead M, Simpson-Herren L, Alley MC. Human tumor xenograft models in NCI drug development. In: Teicher BA, editor. Anticancer drug development: preclinical screening, clinical trials and approval. Totowa, NJ: Humana Press; 1997. p. 101–25.
42. Alley MC, Hollingshead MG, Dykes DJ, Waud WR. Human tumor xenograft models in NCI drug development. In: Teicher BA, Andrews PA, editors. Anticancer drug development: preclinical screening, clinical trials and approval. Totowa, NJ: Humana Press; 2004. p. 125–52.
43. National Research Council. Guide for the care and use of laboratory animals. 8th ed. Washington, DC: National Academies Press; 2011.
44. Houghton PJ, Morton CL, Tucker C, Payne D, Favours E, Cole C, et al. The pediatric preclinical testing program: description of models and early testing results. Pediatr Blood Cancer 2007;49:928–40.
45. Seah VM, Wong KP. 2, 6-Dichloro-4-nitrophenol (DCNP), an alternate-substrate inhibitor of phenolsulfotransferase. Biochem Pharmacol 1994; 47:1743–9.
46. Raftogianis RB, Wood TC, Weinshilboum RM. Human phenol sulfotransferases SULT1A2 and SULT1A1: genetic polymorphisms, allozyme properties, and human liver genotype–phenotype correlations. Biochem Pharmacol 1999;58:605–16.
47. Bendadani C, Meinl W, Monien B, Dobbernack G, Florian S, Engst W, et al. Determination of sulfotransferase forms involved in the metabolic activation of the genotoxicant 1-hydroxymethylpyrene using bacterially expressed enzymes and genetically modified mouse models. Chem Res Toxicol 2014;27:1060–9.

Published OnlineFirst July 24, 2019; DOI: 10.1158/1535-7163.MCT-19-0185

Molecular Cancer Therapeutics

Specific RITA Modification Produces Hyperselective Cytotoxicity While Maintaining *In Vivo* Antitumor Efficacy

Brian D. Peyser, Ann Hermone, Joseph M. Salamoun, et al.

Mol Cancer Ther 2019;18:1765-1774. Published OnlineFirst July 24, 2019.